

SPITZER OBSERVATIONS OF THE SUPERGIANT SHELL REGION IN IC 2574

JOHN M. CANNON¹, FABIAN WALTER¹, GEORGE J. BENDO², DANIELA CALZETTI³, DANIEL A. DALE⁴, BRUCE T. DRAINE⁵, CHARLES W. ENGELBRACHT², KARL D. GORDON², GEORGE HELOU⁶, ROBERT C. KENNICUTT, JR.², ERIC J. MURPHY⁷, MICHELE D. THORNLEY⁸, LEE ARMUS⁶, DAVID J. HOLLENBACH⁹, CLAUS LEITHERER³, MICHAEL W. REGAN³, HÉLÈNE ROUSSEL⁶, KARTIK SHETH⁶

ApJ Letters, in press; Submitted 23 June 2005; Accepted 28 July 2005

ABSTRACT

We present spatially resolved *Spitzer* imaging of the supergiant shell region of the M81 group dwarf galaxy IC 2574 obtained as part of the *Spitzer Infrared Nearby Galaxies Survey*. This region harbors one of the best nearby examples of a kinematically distinct H I shell, with an associated remnant stellar cluster; the shell is initiating sequential star formation as it interacts with the surrounding interstellar medium. This region dominates the infrared luminosity of IC 2574 and is spatially resolved in all *Spitzer* imaging bands. We study the differences in dust temperature as a function of local environment and compare local star formation rates as inferred from H α and total infrared luminosities. We find that the strong H α sources are associated with regions of warm dust; however, the most luminous infrared and H α sources are not necessarily co-spatial. The coolest dust is found in the regions farthest from the rim of the shell; these regions show the best agreement between star formation rates derived from H α and from total infrared luminosities (although discrepancies at the factor of 3–4 level still exist). There is considerable variation in the radio-far infrared correlation in different regions surrounding the shell. The low dust content of the region may influence the scatter seen in these relations; these data demonstrate that the expanding shell is dramatically affecting its surroundings by triggering star formation and altering the dust temperature.

Subject headings: galaxies: dwarf — galaxies: irregular — galaxies: ISM — galaxies: individual (IC 2574) — infrared: galaxies

1. INTRODUCTION

One of the most dramatic effects of vigorous star formation (SF) is the creation of holes and shells in the interstellar medium (ISM). It is commonly proposed that these structures are caused by feedback from massive stars (stellar winds and Type II SNe; e.g., Tenorio-Tagle & Bodenheimer 1988), though alternative scenarios do exist (high velocity cloud impacts, disk instabilities, turbulence, ram pressure stripping; e.g., Sánchez-Salcedo 2002). Starburst regions and sites of massive cluster formation provide spatially and temporally concentrated feedback that can create the largest of these structures. Holes and shells are therefore a direct, observable signature of the deposit of energy from stars into the ISM.

These structures are found in a great variety of environments, from the Milky Way disk (e.g., McClure-Griffiths et al. 2002) to the ISM of dwarf galax-

ies (e.g., Walter 1999). After being formed by the combined effects of SNe and stellar winds, the evolution of holes and shells will have a strong environmental dependence; in normal spiral disks, these structures are erased by turbulent motions and rotational shear on time scales of $\sim 10^7$ yr. On the other hand, in dwarf galaxies (typically displaying solid-body rotation), rotational shear will not play a major role, and holes and shells may remain coherent until pressure equilibrium is re-established with the local ISM (e.g., Elmegreen & Hunter 2000). Indeed, studies of active, nearby dwarf galaxies show that these systems are permeated with holes and shells to the H I resolution limit [e.g., the Large Magellanic Cloud (Kim et al. 1999); the Small Magellanic Cloud (Stanimirovic et al. 1999); and IC 10 (Wilcots & Miller 1998), to name just a few].

IC 2574 is a comparatively large (optical disk ~ 18 kpc diameter), relatively low-metallicity [$12 + \log(\text{O}/\text{H}) \simeq 8.15$, or $\sim 30\% Z_{\odot}$; Miller & Hodge 1996] dwarf galaxy in the M81 group that is undergoing active current SF (H α -derived SFR $\simeq 0.09 M_{\odot} \text{ yr}^{-1}$; Miller & Hodge 1994, Kennicutt 1998). The galaxy hosts a multitude of H I holes and shells (Walter & Brinks 1999), which at the distance of 4.0 Mpc (Karachentsev et al. 2002) provide a unique opportunity to study the process of SF and to observe its effects on the surrounding ISM. The most dramatic “supergiant shell” (SGS; Walter et al. 1998; Walter & Brinks 1999) is expanding at $\sim 25 \text{ km s}^{-1}$, has a diameter of ~ 790 pc, a kinematic age of 15.8 Myr, an H I mass of $\sim 8.2 \times 10^5 M_{\odot}$, and requires an energy input of $\sim 5.8 \times 10^{52}$ erg. As shown in Stewart & Walter (2000), the progenitor stellar cluster is interior to the shell, and the expanding structure is igniting sequential

¹ Max-Planck-Institut für Astronomie, Königstuhl 17, D-69117, Heidelberg, Germany; cannon@mpia.de, walter@mpia.de

² Steward Observatory, University of Arizona, 933 North Cherry Avenue, Tucson, AZ 85721

³ Space Telescope Science Institute, 3700 San Martin Drive, Baltimore, MD 21218

⁴ Department of Physics and Astronomy, University of Wyoming, Laramie, WY 82071

⁵ Princeton University Observatory, Peyton Hall, Princeton, NJ 08544

⁶ California Institute of Technology, MC 314-6, Pasadena, CA 91101

⁷ Department of Astronomy, Yale University, New Haven, CT 06520

⁸ Department of Physics, Bucknell University, Lewisburg, PA 17837

⁹ NASA/Ames Research Center, MS 245-6, Moffett Field, CA, 94035

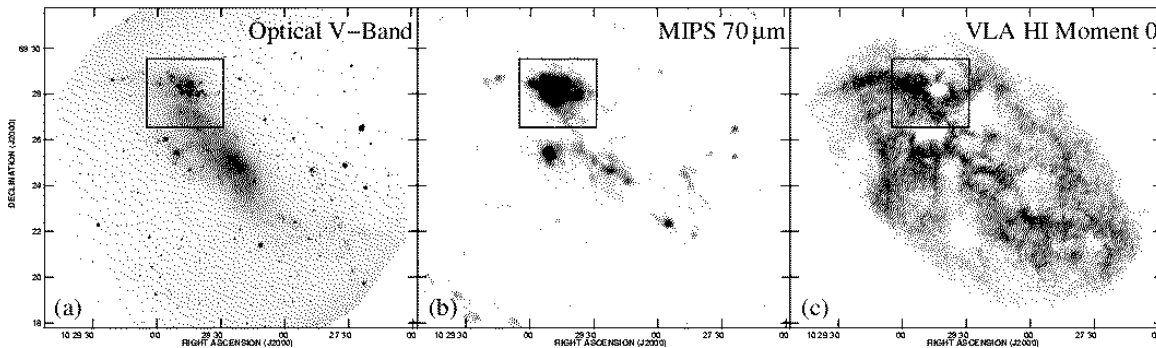


FIG. 1.— Optical V-band (a), MIPS 70 μm (b) and H I (c) images of IC 2574. Note that the SGS region dominates the far-IR luminosity of IC 2574, though emission is associated with other star formation regions. The box in each field denotes the area shown in Figure 2, and is $\sim 4.4 \times 3.8$ kpc at the adopted distance.

SF on the shell rim.

2. OBSERVATIONS AND DATA REDUCTION

For an overview of the *Spitzer Infrared Nearby Galaxies Survey* (*SINGS*) observational strategies, see Kennicutt et al. (2003). IC 2574 was observed for 71 minutes in IRAC mosaicing mode on 28 and 29 October, 2004; MIPS scan mapping mode observations were obtained on 1, 3 November, 2004, for a total of 127.6 minutes. All data were processed by the *SINGS* pipelines. The IRAC pipeline processes basic calibrated data images; flux levels are uncertain at the $\sim 10\%$ level. The MIPS Instrument Team Data Analysis Tool (Gordon et al. 2005) was used to process the MIPS data. Systematic uncertainties (e.g., detector nonlinearities, time-dependent responsivity variations, background removal, etc.) limit the absolute flux calibration to $\sim 10\%$ at 24 μm and to $\sim 20\%$ at 70 and 160 μm . Fluxes were measured after convolution to the ($38''$ FWHM) 160 μm MIPS beam, using kernels derived from observations of a bright star (IRAC) or from STinyTim models, smoothed to match the observed PSFs (assuming a 25 K black body, suitable for the dust temperatures derived; MIPS).

3. MULTIWAVELENGTH EMISSION FROM THE SGS

The SGS region provides the bulk ($\simeq 50\%$ at 24 and 70 μm) of the total IR (TIR) luminosity of IC 2574 at wavelengths longer than ~ 5 μm . In Figure 1 we present a comparison of the total galaxy emission in the optical V band, the MIPS 70 μm band, and the H I spectral line. Note in Figure 1(c) that IC 2574 contains numerous H I shells (Walter & Brinks 1999 identify 48 holes and shells in the ISM; the SGS studied here corresponds to # 35 from that study).

In Figure 2 we present images of the SGS region at nine different wavelengths. Note from the optical (V-band; Figure 2a) and near-IR (IRAC 3.6 μm ; Figure 2b) images that the progenitor stellar cluster lies directly interior to the H I shell (see also Stewart & Walter 2000); this is one of the clearest examples of a kinematically distinct gaseous shell with the parent cluster still visible. By 8 μm (see Figure 2c) the spectral energy distribution of the cluster has fallen below the detection limit, and emission from hot dust and gas dominates; variations in emission in the MIPS bands (Figures 2d, e, f) indicate a wide variety of dust temperatures and spectral energy distributions. Note that the shell morphology is still ev-

ident at 70 and 160 μm ; the diffuse emission in the shell is most likely caused by the MIPS PSF profiles, which spread flux from high surface brightness regions onto arcminute scales (i.e., a few times the MIPS 160 μm PSF FWHM). Comparison of the MIPS, H α and radio continuum images [Figures 2(g, h)] shows a wide variation in the relative ratios. Finally, the H I distribution [Figure 2(i)] shows the H I shell very clearly; it is expanding into a non-uniform medium that may partially explain the variety of dust properties around the shell rim.

Flux densities were extracted in the apertures shown in Figure 2 (see Table 1); these regions were selected to encompass the mid-IR, far-IR, H α , and H I emission peaks with the minimum number of apertures and amount of overlap (note that some apertures contain distinct emission properties at different wavelengths; e.g., SGS1 shows a pronounced difference in H α and radio continuum morphologies). The size of these apertures corresponds to the FWHM ($38'' = 740$ pc) of the MIPS 160 μm beam. Aperture correction factors have not been applied to the values shown in Table 1; the extent of the apertures for all wavelengths up to the MIPS 70 μm band (sampling more than 2, 6, 16, and 36 times the FWHM at MIPS 70 μm , MIPS 24 μm , IRAC 8 μm , and IRAC 3.6 μm , respectively) should imply relatively small aperture correction effects at these wavelengths. There will be some aperture effects at MIPS 160 μm and potentially at 70 μm as well, though the quantification of these factors depends on many parameters (including the distribution of light within the aperture, location and brightness of neighboring sources, and many others).

4. VARYING DUST CONDITIONS IN THE SGS REGION

The characteristics of the dust change dramatically between apertures. There are appreciable variations in the dust temperature; $f_\nu(70 \mu\text{m})/f_\nu(160 \mu\text{m})$ varies by a factor of ~ 3 , with the warmest dust in regions SGS3 and SGS5. Fitting blackbody functions modified by a λ^{-2} emissivity to the 70 and 160 μm MIPS images (see, e.g., Bianchi et al. 1999), these fluctuations correspond to a temperature range of ~ 23 -29 K (averaged over each aperture; see Table 1). Note that the warmest dust is found in regions that have the highest H α flux; the coolest dust is found in region SGS2, which is at the largest distance from the SGS itself, and also shows the lowest H α flux. Interestingly, region SGS4, which shows the highest flux density in all *Spitzer* bands, does not

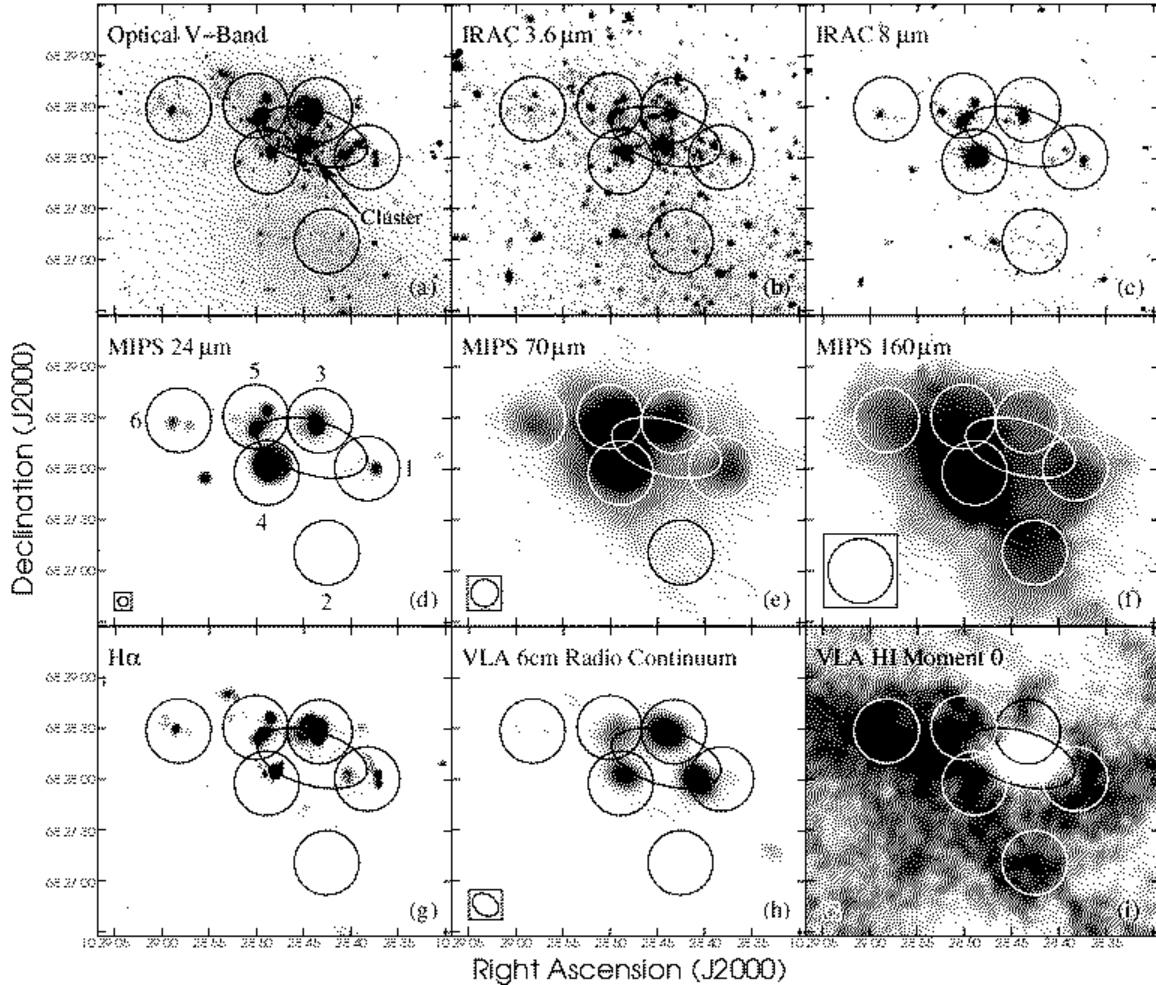


FIG. 2.— Images of the SGS region at nine different wavelengths (see Figure 1 for location): optical V-band (a); IRAC 3.6 and 8 μm (b, c); MIPS 24, 70 160 μm (d, e, f); continuum-subtracted $\text{H}\alpha$ (g); 6 cm radio continuum (h); H I moment zero image. The location of circular apertures SGS 1 - 6 are overlaid, and labeled in (d); the SGS is shown as an ellipse in each frame. In frames (d), (e), (f), and (i), the beam sizes (FWHM) are shown as boxed circles at bottom left.

show the highest $\text{H}\alpha$ flux.

Comparing the far-IR, $\text{H}\alpha$, and H I morphologies, it is evident that all regions except SGS3 occupy areas with high H I surface brightness (H I column densities $\gtrsim 2 \times 10^{21} \text{ cm}^{-2}$). SGS3 is the region with the largest $\text{H}\alpha$ and 6 cm radio continuum fluxes, arguing for strong active SF, and also the highest $f_\nu(70 \mu\text{m})/f_\nu(160 \mu\text{m})$ dust temperature ratio. Given the age of the shell ($\simeq 15 \text{ Myr}$) and the expected lifetimes of H II regions and associated thermal radio continuum emission ($\lesssim 30 \text{ Myr}$), this shell may be initiating rapid SF that quickly disperses the local gas supply.

4.1. Variations in the IR vs. $\text{H}\alpha$ Ratio

In principle, all UV photons within dusty environments will be absorbed and re-radiated in the IR; thus, there should exist a correlation between the IR luminosity and other SFR indicators, such as $\text{H}\alpha$ emission. However, this simple scenario can become complicated in different environments, with dependencies on stellar populations, dust content, etc. (see Kennicutt 1998 for a more detailed discussion). In the case of (typically low-metallicity) dwarf star-forming galaxies such as IC 2574,

the correlation between various SFR indicators may be especially complicated, given their low dust contents and IR luminosities. Dust extinction effects (in both an absolute and differential sense) on the $\text{H}\alpha$ fluxes in the SGS are minimal, based on two independent lines of evidence: first, the UV imaging study of this region by Stewart & Walter (2000) shows typical line-of-sight reddening values in the wavelength range around $\text{H}\alpha$ of $A_R \simeq 0.15 \text{ mag}$, with a maximum of $\sim 0.3 \text{ mag}$; second, new *HST*/ACS imaging and color-magnitude diagram analysis of this region (E.D. Skillman, private communication) easily separates the blue helium-burning and main sequence stars, which at this metallicity are separated by $\simeq 0.2$ magnitudes in (V-I) color.

We find that the $L(\text{H}\alpha)/L(\text{TIR})$ ratio is systematically higher (by factors of ~ 10 ; see Table 1) in regions that are bright in $\text{H}\alpha$ compared to more quiescent regions. If one were to naively convert the $\text{H}\alpha$ and IR fluxes to SFRs [using the relations of Kennicutt (1998) and Dale & Helou (2002)], the $\text{SFR}(\text{H}\alpha)$ values would be systematically higher (by factors of ~ 10) than those derived from the total IR luminosity in the active regions. Since the Kennicutt (1998) FIR calibration assumes complete

TABLE 1
DUST EMISSION AND DERIVED PROPERTIES IN THE IC 2574 SUPER GIANT SHELL^a

Parameter	SGS 1	SGS 2	SGS 3	SGS 4	SGS 5	SGS 6	SGS Total
α (J2000)	10:28:38.275	10:28:42.559	10:28:43.301	10:28:48.912	10:28:50.102	10:28:58.260	10:28:44.1
δ (J2000)	68:28:00.44	68:27:10.98	68:28:28.32	68:27:57.83	68:28:30.76	68:28:28.66	68:28:12.6
H α Flux ^b	37 \pm 6	7.5 \pm 1.3	102 \pm 20	49 \pm 7	57 \pm 9	17 \pm 3	380 \pm 60
H α Convolved Flux ^c	28 \pm 6	8.5 \pm 1.3	66 \pm 20	37 \pm 7	48 \pm 9	12 \pm 3	380 \pm 60
IRAC 3.6 μ m Flux Density	1.4 \pm 0.2	1.6 \pm 0.2	1.9 \pm 0.3	2.0 \pm 0.3	1.8 \pm 0.3	1.1 \pm 0.2	28 \pm 4
IRAC 4.5 μ m Flux Density	1.3 \pm 0.2	1.4 \pm 0.2	1.7 \pm 0.3	1.9 \pm 0.3	1.7 \pm 0.3	1.2 \pm 0.2	29 \pm 4
IRAC 8.0 μ m Flux Density	1.1 \pm 0.2	1.1 \pm 0.2	1.5 \pm 0.2	2.9 \pm 0.4	1.9 \pm 0.3	0.9 \pm 0.1	22 \pm 3
MIPS 24 μ m Flux Density	5.3 \pm 0.8	2.6 \pm 0.4	12 \pm 2	24 \pm 4	15 \pm 2	4.6 \pm 0.7	100 \pm 20
MIPS 70 μ m Flux Density	110 \pm 20	70 \pm 20	160 \pm 30	250 \pm 50	240 \pm 50	97 \pm 20	1900 \pm 400
MIPS 160 μ m Flux Density	150 \pm 40	160 \pm 40	140 \pm 40	290 \pm 70	250 \pm 60	160 \pm 40	2600 \pm 650
6 cm Flux Density	0.63 \pm 0.07	0.046 \pm 0.01	0.88 \pm 0.09	0.53 \pm 0.06	0.50 \pm 0.06	0.13 \pm 0.02	3.03 \pm 0.4
F(H α)/F(TIR)	0.044	0.011	0.090	0.024	0.033	0.021	0.026
F(H α)/F(TIR) ^c	0.034	0.012	0.058	0.019	0.028	0.014	0.026
T _{DUST} (K)	26 \pm 3	23 \pm 3	29 \pm 3	26 \pm 3	28 \pm 3	25 \pm 3	N/A
q (TIR/Radio) ^d	2.55	3.61	2.53	3.01	2.96	3.23	3.11

^aAll values listed in units of mJy, unless otherwise noted. *Spitzer* flux densities were derived without aperture corrections, using images convolved to the MIPS 160 μ m resolution, with foreground stars removed in the IRAC and MIPS 24 μ m bands.

^bDerived from the work of Miller & Hodge (1994); units of 10^{-14} erg sec⁻¹ cm⁻².

^cUsing the H α image convolved to the MIPS 160 μ m FWHM = 38".

^dThe value of q in the radio-far IR relation, derived using the total IR flux and the radio continuum flux at 6 cm. These calculations assume a mix of thermal and nonthermal emission (i.e., $\alpha = -0.7$, where $S_\nu \sim \nu^\alpha$) for the extrapolation from 20 to 6 cm flux densities.

absorption of the starlight, this factor-of-ten difference implies a typical H α extinction in these regions of about 10% ($A(\text{H}\alpha) \sim 0.1$ mag). This is roughly consistent with the range of values cited above, and suggests caution in the application of SFR relations based on total IR luminosities in low-metallicity environments. Note that the variations in the L(H α)/L(TIR) ratio are not due only to varying spatial resolutions between H α and 160 μ m; we tested the severity of this effect by convolving the H α image to the 160 μ m resolution, and find that the L(H α)/L(TIR) ratio still varies by factors of ~ 5 within the SGS region (see Table 1).

4.2. Variations in the Radio-Far IR Correlation

Assuming that the total IR fluxes (derived by applying equation 4 from Dale & Helou 2002) and the radio continuum emission are related via a constant value [$q \propto \log(S_{\text{TIR}}/S_{\text{RC}})$; see, e.g., Bell (2003) for details], we derive strong variations in the value of q(TIR/Radio) throughout the SGS region (see Table 1). The mean value of “q” derived within the SGS region ($\simeq 3.0$) is consistent with, though slightly larger than, the average

global values found in a sample of larger spiral galaxies in the *SINGS* sample (Murphy et al. 2005); we find variations of $\simeq 1$ dex in the value of “q” throughout the SGS region. These strong variations may be a result of the low dust content in IC 2574 (an effect of the low metal content, or of dust destruction in the extreme SGS environment).

5. CONCLUSIONS

We have presented a multiwavelength study of the SGS region in IC 2574, highlighting new *Spitzer* imaging obtained as part of *SINGS*. The unique multiwavelength properties demonstrate that the expanding shell is dramatically affecting its surroundings by triggering SF and by altering the dust temperature and characteristics.

The *Spitzer Space Telescope* Legacy Science Program “The Spitzer Infrared Nearby Galaxies Survey” was made possible by NASA through contract 1224769 issued by JPL/Caltech under NASA contract 1407. The authors thank Evan Skillman for useful discussions, and the anonymous referee for comments that helped to improve the manuscript.

REFERENCES

- Bell, E. F. 2003, ApJ, 586, 794
 Bianchi, S., Davies, J. I., & Alton, P. B. 1999, A&A, 344, L1
 Dale, D. A., & Helou, G. 2002, ApJ, 576, 159
 Elmegreen, B. G., & Hunter, D. A. 2000, ApJ, 540, 814
 Gordon, K. D., et al. 2005, PASP, 177, 503
 Helou, G., et al. 2004, ApJS, 154, 253
 Karachentsev, I. D., et al. 2002, A&A, 383, 125
 Kennicutt, R. C. 1998, ARA&A, 36, 189
 Kennicutt, R. C., et al. 2003, PASP, 115, 928
 Kim, S., Dopita, M. A., Staveley-Smith, L., & Bessell, M. S. 1999, AJ, 118, 2797
 McClure-Griffiths, N. M., Dickey, J. M., Gaensler, B. M., & Green, A. J. 2002, ApJ, 578, 176
 Miller, B. W., & Hodge, P. 1994, ApJ, 427, 656
 Miller, B. W., & Hodge, P. 1996, ApJ, 458, 467
 Murphy, E. J., et al. 2005, ApJ, submitted
 Sánchez-Salcedo, F. J. 2002, Revista Mexicana de Astronomía y Astrofísica, 38, 39
 Stanimirovic, S., Staveley-Smith, L., Dickey, J. M., Sault, R. J., & Snowden, S. L. 1999, MNRAS, 302, 417
 Stewart, S. G., & Walter, F. 2000, AJ, 120, 1794
 Tenorio-Tagle, G., & Bodenheimer, P. 1988, ARA&A, 26, 145
 Walter, F. 1999, Publications of the Astronomical Society of Australia, 16, 106
 Walter, F., & Brinks, E. 1999, AJ, 118, 273
 Walter, F., Kerp, J., Duric, N., Brinks, E., & Klein, U. 1998, ApJ, 502, L143
 Wilcots, E. M., & Miller, B. W. 1998, AJ, 116, 2363